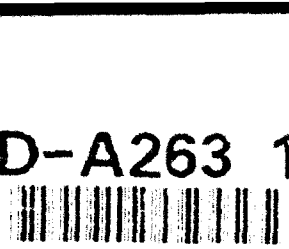

ARMY RESEARCH LABORATORY

Applications of Laser Light Scattering in Polymer Dilute Solution Characterization

Marie Kayser Potts

ARL-TR-85

February 1993

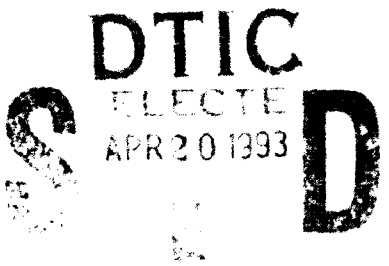

The findings in this report are not to be construed as an official Department of the Army position unless so designated by other authorized documents.

Citation of manufacturer's or trade names does not constitute an official endorsement or approval of the use thereof.

Destroy this report when it is no longer needed. Do not return it to the originator.

REPORT DOCUMENTATION PAGE

Form Approved
OMB No. 0704-0188

1. AGENCY USE ONLY (Leave blank)	2. REPORT DATE	3. REPORT TYPE AND DATES COVERED
	February 1993	Final

4. TITLE AND SUBTITLE
APPLICATIONS OF LASER LIGHT SCATTERING IN POLYMER DILUTE SOLUTION CHARACTERIZATION

5. FUNDING NUMBERS

6. AUTHOR(S)
Marie Kayser Potts

7. PERFORMING ORGANIZATION NAME(S) AND ADDRESS(ES)
U.S. Army Research Laboratory
Watertown, Massachusetts 02172-0001
ATTN: AMSRL-MA-PB

8. PERFORMING ORGANIZATION REPORT NUMBER
ARL-TR-85

9. SPONSORING/MONITORING AGENCY NAME(S) AND ADDRESS(ES)
U.S. Army Research Laboratory
2800 Powder Mill Road
Adelphi, MD 20783-1145

10. SPONSORING/MONITORING AGENCY REPORT NUMBER

11. SUPPLEMENTARY NOTES

12a. DISTRIBUTION/AVAILABILITY STATEMENT
Approved for public release; distribution unlimited.

12b. DISTRIBUTION CODE
A

13. ABSTRACT (Maximum 200 words)

Dynamic light scattering (or photon correlation spectroscopy, PCS) can be used to determine the frequency distribution of the light scattered from polymer solutions. This distribution contains information about the dynamics of the system. Depending on the wavelength of radiation and the size of the polymer molecule, the translations and rotations of the entire molecule, or the motions of the monomers can be studied. This information, combined with static light scattering (the traditional Zimm Plot analysis), can yield a molecular weight distribution (MWD), z-average radius of gyration (R_g), hydrodynamic radius (R_h), translational diffusion coefficient (D_t), and in some cases a rotational diffusion coefficient (D_r). Dynamic light scattering (DLS) has been used extensively in the dilute solution regime to determine the type of information listed above, and the theories associated with the various phenomena are well defined. DLS can also be applied to the analyses of semi-dilute solutions and to study the dynamics of entangled systems (*e.g.*, polymer melts or diffusion of polymer chains in a matrix.), although the interpretation of this type of DLS is still speculative. This report will focus on the use of DLS to determine translational diffusion coefficients, and the combination of static and dynamic light scattering to determine molecular weight distributions.

14. SUBJECT TERMS
Light scattering, molecular weight, solutions, polystyrene

15. NUMBER OF PAGES
29

16. PRICE CODE

17. SECURITY CLASSIFICATION OF REPORT	18. SECURITY CLASSIFICATION OF THIS PAGE	19. SECURITY CLASSIFICATION OF ABSTRACT	20. LIMITATION OF ABSTRACT
Unclassified	Unclassified	Unclassified	UL

NSN 7540-01-280-5500

Standard Form 298 (Rev. 2-89)
Prescribed by ANSI Std. 239-18
298-102

Contents

Figures

Tables

1. Introduction

1.1 Historical Introduction

The initial theory of light scattering by gaseous particles was developed in the late 1800's by Rayleigh, and extended by Mie, Debye and others in the early 1900's. Smoluchowski (1908) and Einstein (1910) developed the fluctuation theory of light scattering which accounted for the decreased scattering by condensed phases due to destructive interference from scattering by different molecules.[1] The application of light scattering to determine the sizes and shapes of polymers came to maturity in the 1940's and 50's, initiated principally by the work of Debye and Zimm.[2] These theories all dealt with the intensity of scattered light, usually measured as a function of a number of scattering angles, i.e., "static" light scattering. Dynamic light scattering on the other hand, is concerned with the frequency distribution of the scattered light. This frequency distribution was first investigated by Brillouin (1914 to 1920) with his discovery of the inelastic component of the light scattered from a simple liquid, caused by scattering from thermal sound waves in the fluid.[1] This "Rayleigh-Brillouin" scattering is characterized by a central Rayleigh peak flanked by a symmetric Brillouin doublet[3] (Figure 1), where the frequency shift of the Brillouin peaks (relative to the central Rayleigh peak) is proportional to the velocity of sound in the fluid, and the linewidth of the Brillouin peak is related to the attenuation of sound in the liquid. Frequency shifts for the Brillouin peak[4] are on the order of 0.01 wavenumbers. Raman spectroscopy, on the other hand, which measures the frequency shifts of the scattered light caused by vibrational motions of the scattering particles, exhibits much larger shifts, typically in the range 4000 - 400 cm^{-1}. The linewidth of the central Rayleigh peak, which is less than 1 MHz (10^{-5} cm^{-1}), is much smaller than either the Raman or the Brillouin shifts. Because the frequencies for the three regimes (Rayleigh line-broadening, Brillouin shifts and linewidths, and Raman shifts) represent such a large energy gap, different detection schemes are needed for each technique. Rayleigh linewidths are generally measured with a digital correlator, using photon counting. Both the frequency shift and the linewidth of the Brillouin peak are determined with a Fabry-Perot interferometer, and the determination of Raman frequency shifts is usually accomplished via a grating monochromator.

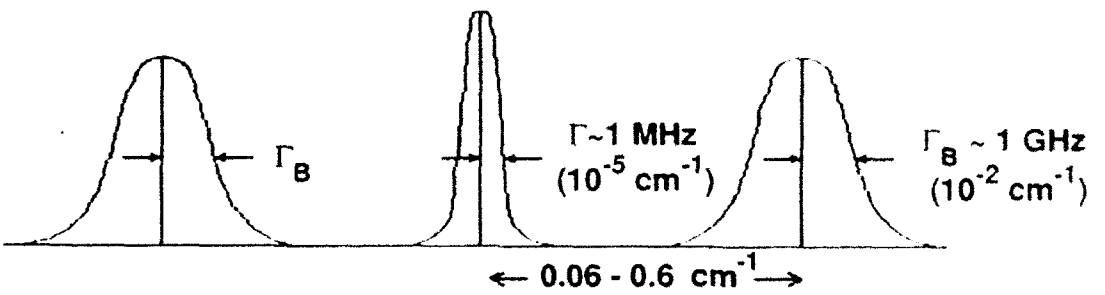

Figure 1. Rayleigh-Brillouin frequency distribution of a fluid

Brillouin spectroscopy does not generally have much application in polymer solution characterization, since the breadth of the Brillouin peaks is very narrow in polymer solutions. Its use in polymer analysis is generally limited to light scattering of bulk polymers (in the melt). The central Rayleigh peak however is broadened by the Brownian motions of polymer molecules in

solution, and contains dynamical information about the polymer solution. The objective of DLS is to extract information on the translational (or rotational) motions of the scattering medium from the linewidth of the Rayleigh scattered light.

1.2 Light Scattering Theory

When an oscillating electromagnetic field (such as in a beam of light) approaches a nonabsorbing, nonionizing material, an oscillating dipole of the same frequency as the nearby electric field is induced in the material. This accelerating dipole then radiates energy of the same frequency in all directions. This is the basis for the phenomenon of light scattering.

Figure 2 shows a schematic view of a typical light scattering spectrometer[5] (dynamic or static). Vertically polarized laser light of incident frequency λ_0 passes through various focusing optics and impinges on a small scattering center in a sample cell. The scattered light at an angle θ (with respect to the exiting beam of the laser) passes through two pinholes to define the coherence area, and is collected via a photomultiplier tube (PMT). The photon pulses are amplified and discriminated and then fed to the digital correlator for analysis. The sample cell is generally surrounded by a vat filled with a liquid whose refractive index closely matches that of the sample cell (*e.g.*, toluene) to limit laser flare at the cell/air interfaces.

Scattering of electromagnetic radiation in a nonconducting, nonmagnetic, nonabsorbing medium occurs as a result of local fluctuations in the dielectric constant (ε) of the medium. The dielectric constant is a vector quantity, and as such, consists of a magnitude and a directional component. A change in either component constitutes a change in the dielectric constant. In a pure liquid, the magnitude of the dielectric constant is the same for all molecules, but the directions of the dielectric constants keep changing due to the Brownian motions of the molecules. Thus, scattering in a pure liquid occurs as a result of the translational motion of the molecules.

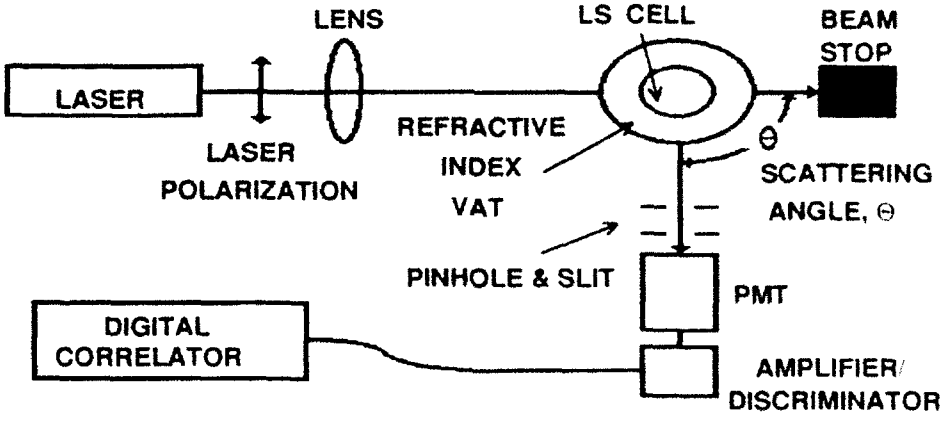

Figure 2. Diagram of light scattering apparatus

1.2.1 Dynamic Light Scattering (DLS)

1.2.1.1 Fluctuations and Autocorrelation Functions

Figure 3 shows an expanded view of a time-dependent signal A(t), similar to what the scattered light intensity from a light scattering experiment might look like: The apparent randomness of

the signal is due to the constant motions of the particles in the scattering region. Over a long enough time period, an average value is obtained, but in the microscopic view, there appear to be random fluctuations in intensity. In this figure, the time axis has been broken up into small sections, Δt (small compared to the period of the fluctuations), and the average value of A, $\langle A \rangle$, is equal to zero (for simplicity). In general, the values of the signal A at two different times, A_j and $A_{j+\tau}$ are different, but if the time increment (Δt) is small enough, then two adjoining sections of the signal, A_j and A_{j+1}, will have values close to each other. Another way of expressing this is to say that A_j and $A_{j+\tau}$ are "correlated" over a small time period, but that the correlation is lost as τ approaches and exceeds the time scale of the fluctuations. The length of time over which the signal is correlated is inherent in the data. The autocorrelation function of a signal, A(t), is expressed mathematically by

$$C(\tau) = \langle A(0)A(\tau) \rangle = \lim_{T \to \infty} \frac{1}{T} \int_0^T A(t)\,A(t + \tau)\,dt\,, \qquad (1)$$

where *dt* is approximately equivalent to the discrete interval Δt described previously. This autocorrelation definition is the description of one point (τ) on the autocorrelation function - it is the sum of a series of multiplications. The entire autocorrelation function is constructed by computing $\langle A(0)A(\tau) \rangle$, for τ ranging from 0 to a point at which the signal is no longer correlated.

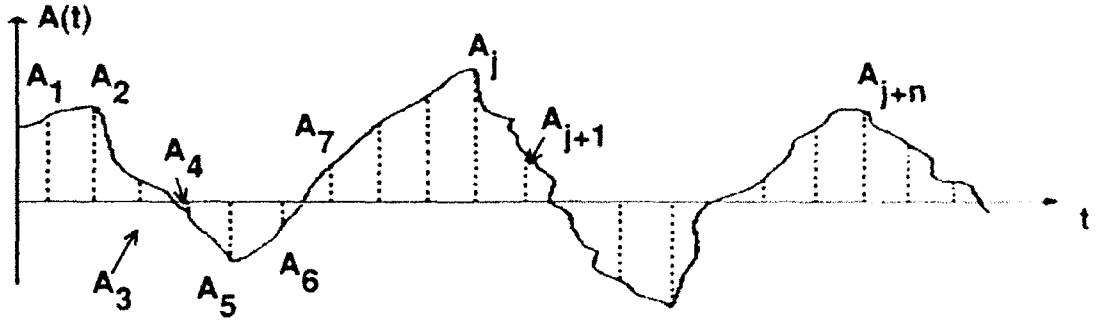

Figure 3. Time-dependent property "A(t)"

Some of the points in Figure 3 are positive, and some are negative; thus the various products computed in Equation 1 will be positive as well as negative (e.g., $A_1 \times A_5$ is negative, but $A_1 \times A_7$, and $A_5 \times A_6$ are positive). The first point of the autocorrelation function is $\langle A(0)A(0) \rangle$, where τ in Equation 1 is replaced by 0. This point is actually the sum of the square of every point along the curve. Since the square of a number is always positive, the first point of the correlation function, $\langle A(0)A(0) \rangle$, will be the largest value in the correlation function, because it will not contain any negative components.

The point $\langle A(0)A(1) \rangle$ can be calculated by shifting the A(t) curve one unit (1 Δt) to the right, and computing the sum of the products of where the two curves overlap. The curves are nearly superimposed, so the value A(0)A(1) will be only slightly less than A(0)A(0), since there are only a few negative products. Eventually, as τ gets large, there is very little overlap between the two curves, and an averaging process takes place, and the correlation function would approach zero (or $\langle A \rangle^2$, if $\langle A \rangle \neq 0$).

The actual correlation function that would be computed from this hypothetical signal A(t), will look essentially like an exponential decay curve (Figure 4 shows an autocorrelation function from a light scattering experiment.) If the correlation function can be described as a single exponential decay, (i.e.,only one physical process is causing the fluctuations), Equation 1 could be simplified to

$$\langle A(0)A(\tau)\rangle = \langle A\rangle \exp\frac{-\tau}{\tau_c} \qquad (2)$$

where τ_c is the characteristic decay time associated with whatever phenomenon is causing the fluctuations in the signal A(t). If the particles diffusing in the medium were all of the same size, they would have the same diffusion coefficient, and a single decay time, τ_c, (related to the diffusion coefficient of the molecules) could be extracted from the curve. However, since macromolecules always have some degree of polydispersity, there will be more than one diffusion coefficient contributing to the autocorrelation function, and the curve actually consists of a superposition of many exponential decay curves.

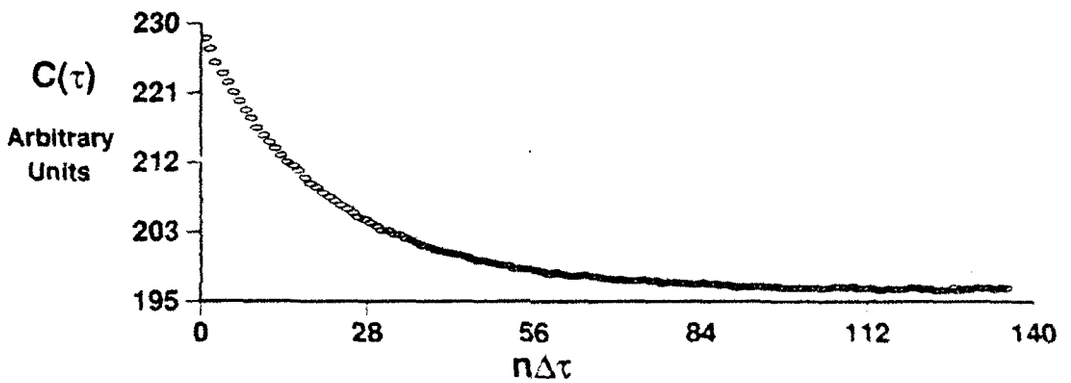

Autocorrelation function measured for sample BR3M (conc. = 0.5035 mg/mL) at scattering angle of 30^{o} and sample time ($\Delta\tau$) = 48 μsec.

Figure 4. Autocorrelation function of scattered light intensity

Since Equation 2 is a function of time, the Fourier transform of this equation should produce an equation in the frequency domain, termed the spectral density, or power spectrum. This is the spectrum of the light scattered by the molecules in solution, as shown in Figure 1, and the linewidth ($\Gamma = 2\pi/\tau_c$), can be extracted from the experimentally determined τ_c. As in the correlation function, this Lawrencian curve is actually a superposition of many Lawrencian curves with different linewidths,, all centered at the incident frequency. The extraction of multiple linewidth from an experimental correlation function will be discussed in Section 1.3.1.

1.2.1.2 Diffusion Coefficients from Autocorrelation Functions

The scattered light intensity, $I_s(t)$, from a solution of macromolecules impinges on a photomultiplier tube which in turn outputs a current, i(t), proportional to $I_s(t)$. Electromagnetic theory tells us that the light intensity is equivalent to the square of the electric field; thus it follows that $I_s(t) = E_s^2(t)) \propto i(t)$. The output of the PMT is fed into a correlator which computes

the intensity autocorrelation function,

$$\langle i(0)i(\tau)\rangle = B\left(|E_s(0)|^2 |E_s(\tau)|^2\right) \qquad (3)$$

where B is a proportionality constant. Equation 3 is a fourth degree correlation function, which is difficult to analyze. In the case of dilute polymer solutions, however, E_s follows a Gaussian distribution, and the correlation function can be simplified to the sum of two correlation functions,[1] the first of which is a constant term, $\langle E_s(0)E_s(0)\rangle^2$ (the baseline of the correlation function), and the second term which is a simpler second degree correlation function, $\langle E_s^*(0)E_s^*(\tau)\rangle^2$, the electric field autocorrelation function.

Incident light which impinges on a molecule with a polarizability tensor α induces a fluctuating dipole moment. The scattered electric field at the detector is proportional to $\alpha_{if}(t)e^{iq\cdot r(t)}$, where $\alpha_{if}(t)$ is the component of the polarizability along the initial and final polarization directions, and the $e^{iq\cdot r(t)}$ factor varies when the molecule translates, where r(t) specifies the molecule's position at time t. The wave vector, q, is equal to $(4\pi n/\lambda)\sin(\theta/2)$, where n is the refractive index of the medium, λ is the wavelength of the incident radiation, and θ is the scattering angle. Thus the electric field autocorrelation function, $\langle E_s^*(0)E_s^*(\tau)\rangle$, is related to the molecular polarizability.

When the product of the wave vector and the radius of the scattering particle is less than unity ($qR << 1$), the time correlation functions are sensitive to fluctuations occurring on a time-scale associated with center-of-mass diffusion.[6] When q is increased (by decreasing the wavelength or increasing the angle) and qR exceeds 1, then internal motions (rotations) of the polymer molecules become important. This is an intermediate q range, and the interpretation of DLS data as due strictly to center-of-mass diffusion can be erroneous. Since the wavelength of light cannot be readily changed, DLS measurements of large particles must be made at low angles to exclude any rotational contributions to the correlation function. Finally, when q gets very large such that qa is on the order of 1, where a is the size of polymer repeat unit, then the time correlation functions are probing motions of the monomers. This requires wavelengths on the order of a few Angstroms, the frequency of neutron radiation, and thus not accessible through light scattering with visible radiation.

If one can assume that the experimentally measured time-correlation function is caused by center-of-mass diffusion, then the diffusion coefficient of the polymer molecule can be simply related to the linewidth via $\Gamma = D_T q^2$. The diffusion constant thus determined can be related to the size of the diffusing particle through the Stokes-Einstein equation,

$$D_T = \frac{k_B T}{6\pi\eta R_h} \qquad (4)$$

where k_B is the Boltzmann constant, T is the temperature, η is the viscosity of the medium the particle is diffusing in, and R_h is the hydrodynamic radius of the particle. For spherical particles (*e.g.* latex spheres) DLS can be used to measure actual particle sizes, however, for dilute polymer solutions, this is really an "equivalent" hydrodynamic radius, with no physical significance.

1.2.1.3 Molecular Weight Distributions from Diffusion Coefficients

Since the time correlation function measured from a DLS experiment contains information on many different linewidths (due to the polydispersity of the polymer sample), abstraction of a distribution of linewidths representative of the different polymer molecules in the sample should be possible. This distribution of linewidths, $G(\Gamma)$, can be transformed to a distribution of diffusion coefficients, G(D), which then can be transformed to a distribution of molecular weights, f(M).

The area under the distribution curve $G(\Gamma)$ is proportional to the time-averaged, total intensity of light scattered at an angle θ (determined from a static light scattering experiment),

$$\langle I(\theta) \rangle = \int_0^\infty G(\Gamma) d\Gamma \quad (5)$$

This time-averaged intensity can also be expressed in terms of the molecular weight components of the polymer species by the following equation[7] from classical light scattering analysis,

$$\langle I(\theta) \rangle = K \sum_i M_i C_i P(\theta, M_i) , \quad (6)$$

where K' contains a collection of optical constants, C_i is the concentration (mass/volume) of a polymer molecule of molecular weight M_i, and $P(\theta, M_i)$ is the particle scattering factor which is different for different shaped molecules (i.e., rigid rods, random coils, etc.).

If C_i can be equated to $f(M_i)\Delta M_i/V$, where $f(M_i)$ represents a molecular weight distribution curve, ΔM_i is a small increment along the curve and V is a unit volume, then the distribution of linewidths can be related to the distribution of molecular weights via

$$G(\Gamma_i)\Delta\Gamma_i = f(M_i)\, M_i\, P(\theta, M_i)\, \Delta M_i . \quad (7)$$

This transformation from gamma-space to molecular weight-space takes place by equating small areas under the $G(\Gamma)$ curve, $\Delta\Gamma$, with area under the f(M) curve, ΔM. The diffusion coefficient has a concentration dependence which can be expressed as

$$D(C) = D_o(1 + k_D C) \quad (8)$$

where k_D is the second virial coefficient for diffusion. D_o can be estimated by extrapolating measured diffusion coefficients at various concentrations to infinite dilution. The diffusion coefficients should also be measured at several angles, particularly for high MW polymers, and extrapolated to zero-angle to exclude any rotational contributions at higher angles. The infinite dilution diffusion coefficient can then be related to a molecular weight via

$$D_o = k_T M^{-b} , \quad (9)$$

where the pre-exponential factor, k_T, depends on the polymer/solvent system, and must be determined experimentally. The exponent b is equal to 0.5 for random coils at the theta condition and has been verified experimentally. For polymers in good solvents b is expected to be closer to 0.6, although experimentally reported values vary from 0.55 to 0.68.[7,8]

If k_D, k_T and b are known (or estimated) then molecular weights can be calculated from experimentally determined linewidths via the following equation

$$M = \left[\frac{k_T q^2 (1+k_D C)}{\Gamma}\right]^{1/b} \qquad (10)$$

where the values of M can be substituted into Equation 7 for the M_i values and the ΔM increments can be calculated by determining the values of M at the endpoints of the $\Delta\Gamma$ increments.

Each M_i in Equation 7 must have a corresponding R_g which is used to determine $P(\theta, M_i)$, and so a radius of gyration is computed for each molecular weight similarly to Equation 9.

$$Rg = k_T' M^{b'} \quad . \qquad (11)$$

Like b, the exponent b' is expected to be around 0.6 for random coils in a good solvent, but not necessarily equivalent to the dynamic exponent b. The pre-exponential k_T' depends on the particular chemical system. For random coil molecules, the particle scattering factor usually takes the form

$$P(X,M) = \frac{2}{X^2}\left[e^{-X} - 1 + X\right] \qquad (12)$$

where $X = q^2 R_g^2$, and R_g is the radius of gyration computed from Equation 11. By combining the results of static and dynamic light scattering measurements with estimates of k_T, k'_T, b, and b', an iterative process can be used to determine an effective molecular weight distribution.

As can be seen from the preceding discussion, much information about the polymer-solvent system must be known in order to determine a molecular weight distribution in this manner. Additionally, most of the equations apply strictly to monodisperse species, and any breadth to the molecular weight distribution adds complications. For these reasons, this method of determining a molecular weight distribution is not of general utility but in certain instances, may be appropriate.

Size exclusion chromatography (SEC) is an experimentally simpler method of determining molecular weight distributions, but has several limitations. SEC requires the use of polymer standards to determine actual molecular weight values, and well-characterized standards are only available for very common polymers. Light scattering, however, is an absolute technique and requires no standards. Additionally, certain polymers may only be soluble in solvents which are incompatible with the chromatography columns, or at temperatures not accessible by ordinary SEC instrumentation. For example, aromatic polyamides such as Kevlar, and poly(aryl ether ketones) are generally soluble only in strong acids. Corrosive solvents are not a problem for light scattering which is usually measured in a glass or quartz cell.

1.2.2 Static Light Scattering (SLS)

Classical electromagnetic theory and solution thermodynamics[9] show that the intensity of light scattered (from a polarized light source of wavelength λ) by small (compared to λ), isotropic scatterers at an angle θ can be represented by

$$\frac{Kc}{R_\theta} = \frac{1}{M_w} + 2A_2 c + 3A_3 c^2 + \ldots \qquad (13)$$

The Rayleigh ratio, R_θ, contains the pertinent measured quantities, and is equal to $I_\theta r^2 / I_o$, where I_θ is the measured scattered light intensity, I_o the incident intensity, and c is the concentration of the solution (mass/volume). Other parameters are grouped into the optical constant K, defined as $4\pi^2 n^2 (dn/dc)^2 / (L\lambda^4)$, where n is the refractive index of the medium, dn/dc (the refractive index increment) is the change in refractive index of the solution with concentration, and L is Avogadro's number. (In practice, the scattering distance r and the incident intensity I_o are not measured. Instead, a solvent for which this Rayleigh ratio has been previously determined [toluene or benzene, typically] is used as a calibration liquid. Its scattered intensity is measured, and the known value of its Rayleigh ratio is used to calculate the values of r and I_o for the current system.)

Equation 13 shows the concentration dependence of the scattered light intensity of a polymer solution. For large ($r > 1/20\ \lambda$) molecules, there is also an angular dependence of the scattered intensity due to the size of the molecule. Small scatterers have a symmetric scattering pattern about $\theta = 90^\circ$, because they look like a point to the incident radiation. Large particles, however, will scatter radiation from different portions of their molecule, and thus there will be destructive interference at the detector due to the phase differences of light arriving at the detector which has scattered from two different points on the same molecule. The scattered light intensity will be highest at large angles, because the difference in path length is larger, and this assymmetry about 90° is used to extract size information.

The angular dependence of the scattered light intensity takes the following form - the ellipsis indicates that higher order terms in $R_g^2 \sin^2(\theta/2)$ are present.

$$\frac{Kc}{R_\theta} = \frac{1}{M_w} \left(1 + \frac{16\pi^2}{3\lambda^2} R_g^2 \sin^2\left(\frac{\theta}{2}\right) + \ldots \right) \qquad (14)$$

For high molecular weight polymers with large radii, the curvature in Equation 14 can be significant, and thus the initial slope must be used to obtain accurate values of M_w and R_g. Equations 13 and 14 can be combined and the molecular weight, second virial coefficient, and the radius of gyration can be obtained from a single plot, to be described in section 1.3.2. The molecular weight determined is absolute (i.e., independent of the solvent used), and is the weight-average value, as opposed to the number-average M_n determined from colligative property measurements. The second virial coefficient is a measure of the thermodynamic interaction of the solute and solvent (the third virial coefficient is usually small and not important unless the solution concentration is high). The radius of gyration determined from light scattering measurements, defined as the root mean square distance of the segments of the molecule from its center of mass, is a z-average value. The size of the molecule and the second virial coefficient are not absolute values, but depend on the solvent used. A_2 is positive for a thermodynamically good solvent (polymer-solvent affinity is greater than polymer-polymer affinity), at 1 varies in magnitude for different solvent qualities, is negative for a poor solvent, and zero (equal affinities) at the theta condition. Accordingly, the radius of gyration is largest in a good solvent, smallest in a poor solvent, and an intermediate value in a theta solvent.

1.3 Data Analysis

1.3.1 Dynamic Light Scattering

In dynamic light scattering experiments, there are two autocorrelation functions of interest: the intensity autocorrelation function $g^{(2)}(\tau)$, which is the function actually computed by the correlator (Equation 3), and the electric field autocorrelation function, $g^{(1)}(\tau)$, which is related to the molecular parameters, described in section 1.2.1.2. These two correlation functions are related through the Siegert relation,

$$g^{(2)}(\tau) = 1 + \beta [g^{(1)}(\tau)]^2 \qquad (15)$$

where the baseline of the experimental correlation function (A) has been subtracted. The constant β, $0 < \beta < 1$, is usually determined as a parameter during the fitting of the data. The electric field correlation function, $g^{(1)}(\tau)$, is assumed to be in the form of a sum of single-exponentials,

$$g^{(1)}(\tau) = \int_0^\infty G(\Gamma)\, e^{-\Gamma\tau}\, d\Gamma \qquad (16)$$

where the Γ's represent the different linewidths due to the different molecular weight species and $G(\Gamma)$ represents their distribution function. As mentioned in sections 1.2.1.2, in the absence of internal motions, the diffusion coefficient is related to the linewidth via

$$\Gamma = D_T q^2. \qquad (17)$$

The goal of any light scattering data analysis routine, therefore, is to invert Equation 16 to obtain $G(\Gamma)$. There are many mathematical methods available for this transformation - a few methods[10] which are available on the Brookhaven instrument will be reviewed briefly. All of the methods described here are least-squares fits, in which the objective function to be minimized is,

$$\chi^2 = \sum_{I=1}^{N} [\, y_m(I\Delta\tau) - y^*(I\Delta\tau)]^2 \qquad (18)$$

where $y_m(I\Delta\tau)$ is the measured correlation function (with the baseline A subtracted) and $y^*(I\Delta\tau)$ is the model correlation function proposed by the particular method of data analysis. The index I runs over all the data points in the correlation function (in the Brookhaven correlator, there are 128 data channels). Equation 18 is minimized with respect to a number of parameters a_j ($j = 1, 2, \ldots, M$), which vary for the different methods of data analysis.

1.3.1.1 Method of Cumulants

The method of cumulants[11] is the simplest way to analyze DLS data, but also yields the least amount of information. Only the average linewidth and its variance can be obtained (the first and second cumulants) with any degree of accuracy. (Sometimes the 3rd cumulant is also reported.) The cumulants are defined in terms of moments about the mean linewidth, where the

m^{th} moment is defined as

$$\mu_m \equiv \int_0^\infty G(\Gamma)(\Gamma - \bar{\Gamma})^m d\Gamma \qquad (19)$$

and the resulting computed correlation function is

$$y^*(\tau) = (A\beta)^{1/2} exp\left(-\bar{\Gamma}\tau + \frac{1}{2!}\mu_2\tau^2 + \cdots\right) \qquad (20)$$

where the ellipsis indicates that higher cumulants may be included. The parameters used to minimize Equation 18 are the cumulants (Γ, μ_2, etc.) and the factor $A\beta$.

1.3.1.2 Exponential Sampling

Another common data analysis routine used in DLS is the Exponential Sampling Technique, also called the LaPlace Transform Inversion,[12] which is based on the eigenfunctions $\psi_\omega(\Gamma)$ and eigenvalues λ_ω of the LaPlace transform of $G(\Gamma)$,

$$\int_0^\infty \psi_\omega(\Gamma) exp(-\Gamma\tau) d\Gamma = \lambda_\omega \psi_\omega(\tau) \qquad (21)$$

where analytical expressions for λ_ω and $\psi_\omega(\Gamma)$ are given in Reference 12.

The distribution function $G(\Gamma)$ is then expanded into its complete set of eigenfunctions via

$$G(\Gamma) = \int_{-\infty}^{\infty} a_\omega \psi_\omega(\Gamma)\, d\omega \,. \qquad (22)$$

By substitution of Equation 22 into Equation 16 and using the relationship in Equation 21, the correlation function can be written as

$$g^{(1)}(\tau) = \int_{-\infty}^{\infty} \lambda_\omega a_\omega \psi_\omega(\tau)\, d\omega \,. \qquad (23)$$

As ω gets very large ($\omega > \omega_{max}$), the eigenvalues approach zero, and their contribution to the correlation function cannot be distinguished from experimental error, thus the distribution of linewidths is band-limited by changing the limits in Equation 22 from $\pm\infty$ to $\pm\omega_{max}$. After a series of mathematical manipulations, $G(\Gamma)$ may be represented as a series of exponentially spaced samples in Γ-space, with amplitudes a_m. The amplitudes are used to minimize Equation 20, with the proposed correlation function given by

$$y^*(I\Delta\tau) = \sum_{m=1}^{M} a_m exp(-\Gamma_m I\Delta\tau) \qquad (24)$$

The best fits to the data are usually obtained with ω_{max} greater than about 3.

1.3.1.3 Non-negatively Constrained Least Squares

This data analysis routine is an adaptation of the previous method, developed for multimodal linewidth distributions.[13] Equation 24 is used, and each a_m is constrained to be non-negative. In this method, the smallest and the largest linewidths (Γ_{min} and Γ_{max}) are predefined to be

functions of the experimental sample time and the average linewidth determined from the slope of the logarithm of the measured data, $y_m(I\Delta\tau)$. In the Brookhaven version of this data routine, the user is given the option of overriding the default Γ_{min} and Γ_{max} values.

1.3.1.4 Double Exponential

This method forces the correlation function to be composed of two discreet exponential functions,[14] as shown in the following equation.

$$g^{(1)}(\tau) = A_1 \exp(-\Gamma_1 \tau) + A_2 \exp(-\Gamma_2 \tau) \qquad (25)$$

This is a dangerous method for analyzing correlation functions unless the user is certain of the bimodal character of the data, because any noise in the data could be interpreted as another species. This type of data analysis is primarily used in DLS of entangled systems, where a fast cooperative diffusion mode of a network, and a slower self-diffusion mode of a smaller unit is present.[15]

1.3.2 Static Light Scattering

For dilute solutions, the measured scattered light intensity from a given illuminated area (the scattering volume) is the superposition of the scattered light intensities from all elements within that region. Thus, the scattered light measured from a solution of polymer molecules consists of the light scattered by the small solvent molecules plus the scattering from the large polymeric species. If the scattering of the pure solvent is measured separately, it can be subtracted from the solution scattering and the scattering due to the polymer molecules alone can be isolated. The resulting excess scattered intensities are converted to Rayleigh ratios, as described in section 1.2.2. The data is usually analyzed via a Zimm Plot in which the (KC/R_θ) values are plotted on the y-axis versus $(\sin^2(\theta/2) + kc)$ on the x-axis, where k is an arbitrary constant used to spread out the points on the plot. The set of points corresponding to the same concentration (different scattering angles) should form a straight line parallel to the other concentrations. Another set of parallel lines (usually with smaller slopes) can be drawn by connecting the points corresponding to a given scattering angle at different solution concentrations. These two sets of parallel lines form a grid-like structure (see Figure 5).

The constant concentration lines can be extrapolated to a "zero-angle" point (with an x-coordinate equal to kc). Likewise, the constant angle lines can be extrapolated to a "zero-concentration" point (with an x-coordinate equal to $(\sin^2(\theta/2))$. Each of the extrapolated "zero-angle" points can be extrapolated to zero-concentration (x value equal to 0); similarly the extrapolated "zero-concentration" points can be extrapolated to zero angle (x value equal to 0), and these two doubly extrapolated lines should intersect at the same point on the y-axis, the reciprocal of the molecular weight. The second virial coefficient is obtained from the initial slope of the zero-angle line (see Equation 13) and the radius of gyration is abstracted from the initial slope of the zero-concentration line (Equation 14). The initial slopes of both of these lines must be used, as higher order terms become significant as concentration and angle increase. The curvature of the zero-angle line should be negligible, unless the solutions are too concentrated, but the curvature of the zero-concentration line can be significant, particularly for large polymeric species. A variation of the Zimm Plot used for analyzing high molecular weight samples, was proposed by Berry,[16] is to plot $(KC/R_\theta)^{1/2}$ values on the ordinate vs. the same abscissa values.

The intercept then yields the reciprocal of $(M_w)^{1/2}$, and the equations for determining A_2 and R_g are slightly different.

The larger the difference in scattered intensity between the solvent and solution, the greater the precision of the parameters determined from the light scattering experiment. The increase in scattering intensity of the polymer solution over that of the pure solvent (at constant measuring angle) depends on four factors: (1) the polymer molecular weight, (2) the concentration of the polymer solution, (3) the difference in the refractive index between the solvent and the polymer solution, and (4) the wavelength of the laser. The polymer molecular weight is obviously fixed, but the other parameters can be adjusted to increase the scattering intensity for a poor scatterer. Increasing the solution concentration (being careful to remain in the dilute solution regime), changing the solvent to one with a larger dn/dc value for the particular polymer, and decreasing the wavelength of the laser, all increase the scattering intensity.

2. Experimental

2.1 Sample Preparation

Table 1. Polymer samples specifications

	Mw x 10^6	Mw/Mn	Composition
N170K	0.168	1.04	100% PL #20137-2
N770K	0.765	1.04	100% PL #20140-9
	0.990	1.04	100% PL #20141-5
	1.53	1.06	100% PL #20142-5
N2M	2.14	1.06	100% PL #20143-2
	2.28	1.05	100% PL #20143-7
N3M	2.91	1.04	100% PL #20145-9
	4.06	1.06	100% PL #20146-6
	9.35	1.20	100% PL #20148-3
BR2M	1.85**	1.2*	47% PL #20142-5, 53% PL #20143-2
BR3M	3.17**	1.2*	56% PL #20143-7 44% PL #20146-6
BI850K	0.839**	2.0*	66% PL #20137-2, 34% PL #20143-2
BI4M	4.08**	2.0*	63% PL #20141-5, 37% PL#20148-3
*Estimated values of M_w and M_w/M_n			

Polystyrenes (PS) with three types of molecular weight distributions (narrow, broad, and bimodal) were investigated to demonstrate the capabilities of dynamic and static light

scattering. Several commercial PS standards from Polymer Laboratories were used individually, and in various combinations and their properties are listed in Table 1. Four standards (N170K, N770K, N2M, and N3M) were used as is for the narrow MW distrubtion samples. Two broad distributions (BR2M and BR3M) and two bimodal distributions (BI850K and BI4M) were simulated by mixing PS standards with similar and dissimilar molecular weights, respectively.

Stock solutions of concentration approximately 1.0 mg/mL of polystyrenes were prepared with toluene (EM Science, spectroscopic grade), and allowed to dissolve at room temperature, with slight agitation, for at least 24 hours. These stock solutions were diluted to three or four concentrations of 0.1 - 0.5 mg/mL for static light scattering experiments, except for the lowest molecular weight samples in which the highest concentrations were about 1.0 mg/mL. Concentrations used in dynamic light scattering were slightly higher - about 0.5 to 1.0 mg/mL.

2.2 Instrumentation

All light scattering measurements were made on a Brookhaven Instruments BI200SM goniometer and BI2030AT 128 channel correlator using a Melles Griot 5 mW helium-neon laser (633 nm) as the light source. The refractive index increment (dn/dc) of PS in toluene was not measured, but a literature value[17] of 0.107 mL/g was used. Toluene was also used as the calibration liquid, with a Rayleigh ratio[18] of 1.41×10^{-5} cm^{-1}. Solvent and polymer solutions were filtered through 0.2μ and 0.45μ PTFE filters, respectively. The temperature of the light scattering cell was maintained at 25.0 ± 0.1 C for all measurements.

3. Results and Discussion

3.1 Static Light Scattering

Static light scattering measurements were made at angles 30°, 37.5°, 45°, 60°, 75°, 90°, 105°, 120°, 135°, 142.5°, and 150° on the eight polymer solutions described in the previous section. The static LS parameters are listed in Table 2 along with the data analysis method used.

Figure 5 shows typical Zimm and Berry plots obtained for different polystyrene samples. The lower molecular weight samples showed a linear concentration dependence and thus were best analyzed through a classical Zimm plot approach, however, a curvature to the fixed concentration data was observed for $M_w > 1.0 \times 10^6$, and thus a Berry plot gave a better fit to the data.

Table 2. Static light scattering parameters

	10^{-6} x M_w g/ mol	R_g, nm	10^{4} x A_2 ml mol/g^2	Type of Plot*
N170K	0.178 0.168	15.9** --	4.97 4.47	Zimm Debye
N770K	0.731	36.6	4.00	Zimm
BI850K	0.729	63.4	0.537	Zimm
BR2M	1.94	70.7	2.52	Berry
N2M	2.21	74.7	2.44	Berry
BR3M	3.01	91.6	2.14	Berry
N3M	3.07	89.8	2.24	Berry
BI4M	3.49	129.8	1.83	Berry

*Zimm Plot: linear fit to concentration and angular data;
Debye Plot: linear fit to 90^0 data only;
Berry Plot: second degree fit to concentration, linear fit to angular data..
**Less than the theoretical lower limit of detection of $R_g = \lambda_o/20 = 32$ nm.

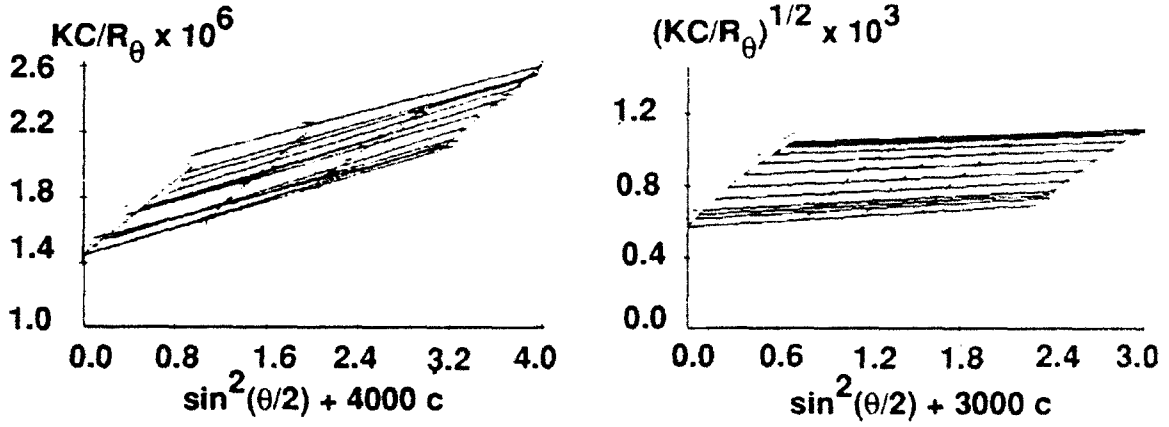

Zimm Plot (left) for N770K (conc. = 0.2505, 0.5010, and 0.7515 mg/mL); and Berry Plot (right) for N3M (conc. = 0.1007, 0.2014, 0.3021, and 0.5035 mg/mL).

Figure 5. Typical Zimm and Berry Plots

The R_g and A_2 values for the unimodal PS samples were linear with molecular weight in log-log plots as can be seen from Figure 6. The relationships derived from these log-log plots are

expressed mathematically by the following equations:

$$R_g = 9.63 \times 10^{-3} M_w^{0.612}, \text{ and } A_2 = 1.78 \times 10^{-2} M_w^{-0.291} \qquad (20)$$

The pre-exponent in the R_g expression is consistent with values in the literature[19-24] (9.196 x 10^{-3} to 1.57 x 10^{-2}) for PS/toluene solutions, although there seem to be two sets of values clustered around 1.0 x 10^{-2} and 1.5 x 10^{-2}. The same references report a range of exponent values from 0.623 to 0.579, which is consistent with the result reported here and the expected theoretical value of 0.6 (section 1.2.1.3), but again the values seem to cluster around two values of 0.58 and 0.61.

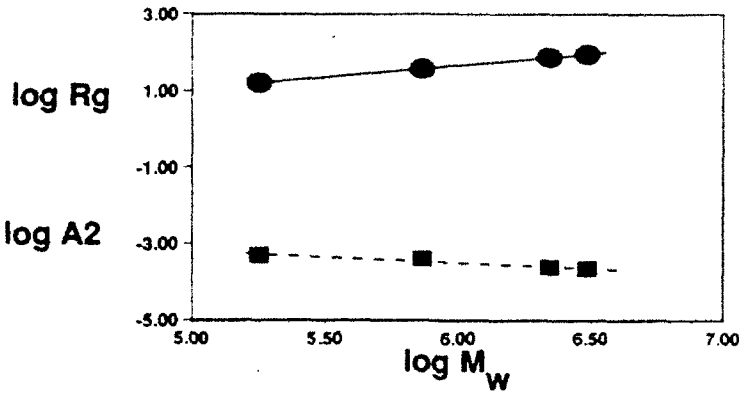

$\log_{10} R_g$ (circles) and $\log_{10} A_2$ (squares) as a function of $\log_{10} M_w$, for samples N170K, N770K, N2M, and N3M.

Figure 6. Plot of log R_g and log A_2 versus log M_w

The A_2 relationship reported here is also in agreement with others[20,22,23] in which the pre-exponential factor ranges from 0.0158 to 0.0281, and the corresponding exponents from -0.286 to -0.329. There were two reported relationships[19,21] with significantly smaller pre-exponential factor and exponents: $A_2 = 0.00636\ M^{-0.225}$; and $A_2 = 0.00436\ M^{-0.203}$. Both report measurements made at 20°C, which would correspond to smaller A_2 values,[25] but one of the other references[20] which was in agreement with the present work was also at 20°C, so there doesn't appear to be a clear correlation with temperature. The latter two expressions come closer to the theoretical exponent of 0.2, predicted by the two-parameter theory.[26]

3.2 Dynamic Light Scattering

Dynamic light scattering measurements were made on all samples except N170K. (For the laser employed in this study, the scattered light intensity from a low MW sample such as N170K is too low to obtain a good correlation function.) A typical correlation function for sample BR3M is shown in Figure 4. The DLS data were obtained for two purposes: (1) to extract infinite dilution values of the diffusion coefficients (D_o) for unimodal samples so that kT and b values from Equation 9 could be evaluated, which are needed for molecular weight distribution transformation, and (2) to see if the particle size distrubution (PSD) data analysis routines from Brookhaven Instruments (BIC) could differentiate between unimodal narrow, unimodal broad, and bimodal distrubutions.

3.2.1 Diffusion Coefficients

Autocorrelation functions measured at a given scattering angle and solution concentration yield an average linewidth, Γ, which can be converted to a diffusion coefficient via Equation 17. For monodisperse systems, this extrapolated diffusion coefficient should be independent of the scattering angle, through the q^2 correction. This angular independence was verified experimentally for sample N3M, and thus diffusion coefficients were measured at one or two angles, and the values averaged. The diffusion coefficients were also measured as a function of concentration for samples BR2M and N3M, and values of k_D (Equation 8) were determined to be 227 and 294 mL/g, respectively. The k_D values determined in this study are consistent with literature values for PS/Toluene solutions, as shown in Figure 7. There doesn't seem to be any theoretical basis

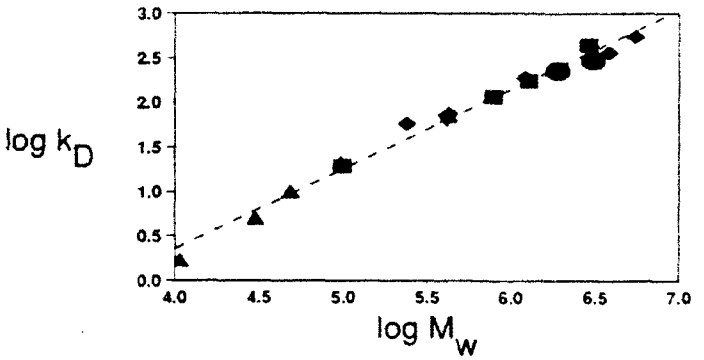

Plot of $\log_{10} k_D$ vs. $\log_{10} M_w$ for this work (●); Ref. 20 (■); Ref. 21 (▲); Ref. 23 (◆); and Ref. 27 (▼). Dotted line is the best fit to all data.

Figure 7. Plot of log k_D versus log M_w

for plotting the log of molecular weight versus the log of k_D; however, a reasonable correlation is obtained which allows extrapolation of k_D values for samples in which a concentration dependence was not measured.

Values of the infinite dilution diffusion coefficient (D_0), the k_D value used to convert D(c) to D_0, the hydronamic radius (R_h) determined from D_0 via Equation 4, and $\rho = Rg/R_h$ are presented in Table 3.

The diffusion coefficients for the unimodal (narrow and broad) MWD polymers were determined from a single exponential fit to the autocorrelation function, which yielded an average Γ, which was then converted to D via $D=\Gamma q^2$. The diffusion coefficients were converted to infinite dilution values using either a measured k_D value or a value extrapolated from Figure 7, based on the M_w determined from static light scattering.

The analysis of the bimodal samples was more indirect, because they were analyzed using the double exponential fitting procedure, which yields particle diameters, not linewidths. Two diameters were obtained from the data analysis, and were converted to diffusion coefficients via the Stokes-Einstein equation. The two diffusion coefficients for each bimodal sample were converted to D_0 values using a single k_D value (from Figure 7, based on the M_w determined from static light scattering) and the total solution concentration. Using average M_w and k_D values for a bimodal system is a rough approximation, however an alternate approach is to use k_D values appropriate for each component, coupled with the concentration of that component.

This analysis yielded similar results. Probably the most realistic approach would be to calculate an effective concentration of each component (which is less than the overall concentration, but more than the indivudual concentration), to be used with the k_D value associated with the particular molecular weight involved. Needless to say, the D_o and the R_h values obtained for the bimodal samples are very approximate, but are included for comparison.

Table 3. Dynamic light scattering parameters

	10^7 x Do', cm^2sec^{-1}	k_D, cm^3g^{-1}	R_h, nm	ρ (= R_g/R_h)
N770K	1.663	105*	23.9	1.531
BR2M	0.9155	227 (251*)	43.35	1.631
N2M	0.8698	282*	45.63	1.637
BR3M	0.7104	294** (372*)	55.87	1.640
N3M	0.7094	294 (378*)	55.94	1.605
BI850K	2.874 0.7568	105*	13.6 51.50	1.173 1.373
BI4M	1.766 0.3371	424*	22.1 115.6	1.987 1.582

*estimated via Figure 7
**measured for sample N3M

The D_o values from the narrow and the broad distributions are plotted against molecular weight in a log-log plot in Figure 8. The two broad distribution samples appear to follow the linear relationship of the narrow distribution polymers. The R_h values from Table 3 can be plotted similarly with molecular weight (not shown here), although since the radii are calculated directly from the diffusion coefficients, the data is not really independent. The dynamic relationships derived from these plots are

$$D_o = 3.18 \times 10^{-4} M^{-0.563} \quad . \textit{and} \quad R_h = 7.68 \times 10^{-3} M^{0.596} . \qquad (27)$$

The pre-exponential factor for the diffusion relationship reported here is a bit smaller than most of the literature values[19-21,27,28] which range from 3.4 - 3.7 x 10^{-4}, although one value[22] is even smaller at 2.29 x 10^{-4}. The absolute value of the exponent in this diffusion relationship is also smaller than those reported for the same references (0.577 - 0.587), with the same exception that Seery *et al.*[22] reported an even lower value of 0.533.

Two papers[23,24] report R_h relationships with larger pre-exponential factors (0.0131 and 0.0103) and smaller exponents (0.560 and 0.577, respectively). The two effects counteract each other somewhat, so overall, the data may not be that different.

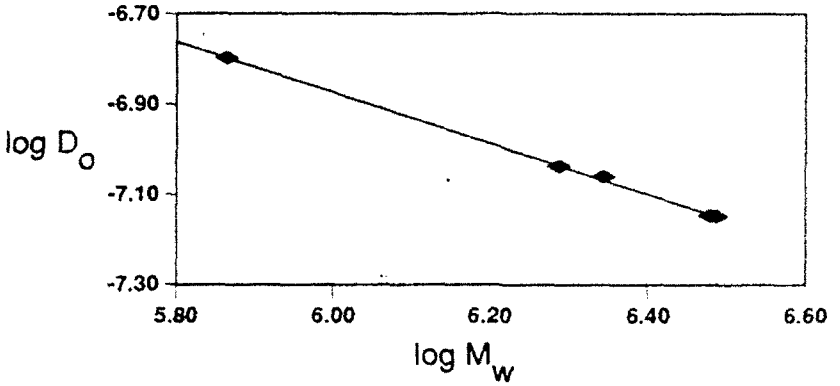

Plot of $\log_{10} D_o$ versus $\log_{10} M_w$ for samples N770K, N2M, N3M, BR2M, and BR3M.

Figure 8. Plot of log D_o versus log M_w

The ρ data in Table 3 are reasonably constant (average ρ = 1.603) except for the bimodal samples, in which both R_g and R_h are very approximate. (The R_g values for the bimodal samples were determined from Equation 26, using either a M_w determined from static light scattering, or the manufacturer's M_w.) This value of 1.603 is in good agreement with the literature: Park *et al.*[24] report a value of 1.59, while 1.6 and 1.5 can be deduced from the data of Appelt and Meyerhoff[19] and Varma,[23] respectively. The theory regarding whether ρ should be a constant value for all polymers in good solvents is unclear.[24]

3.2.2 Particle Size Distribution Analysis

Autocorrelation functions measured for the narrow distribution samples N770K, N2M and N3M were analyzed by the various particle size distribution (PSD) analysis routines described in section 1.3.1. The results were consistent in that unimodal narrow distributions were obtained. The double-exponential analysis was either not available as an option (the experimental data could not be fit to a double exponential) or a double exponential fit would yield a major peak (~99%) at the expected particle diameter and a very minor peak at an unrealistic (either too small or too large) diameter. The peak diameter and the breadth of the distribution were invariant with the type of baseline, the number of data points, and the method of data anlysis used. A typical distribution is shown in Figure 9a.

Similar results were obtained for the broad distribution samples (see Figure 9b), although there was considerable variation in the breadth of the distributions determined. The data analysis routines do not appear to be sensitive enough to distinguish between a narrow and a moderately broad distribution. The distributions computed for a narrow and a broad molecular weight sample of approximately the same molecular weight (shown in Figures 9a and 9b, respectively), appear to have equal breadth. Due to the low power laser employed in this study, and the necessity of keeping the solution concentrations below the overlap concentration, c*, the scattering

intensity for all correlation functions was very low. Data had to be accumulated for long periods of time (30-60 minutes) to obtain smooth correlation functions. Possibly, smoother data would produce more consistent results, but in general, the technique of DLS is not suitable for obtaining detailed information about size distributions (see, for example, Ref. 5, 10-14).

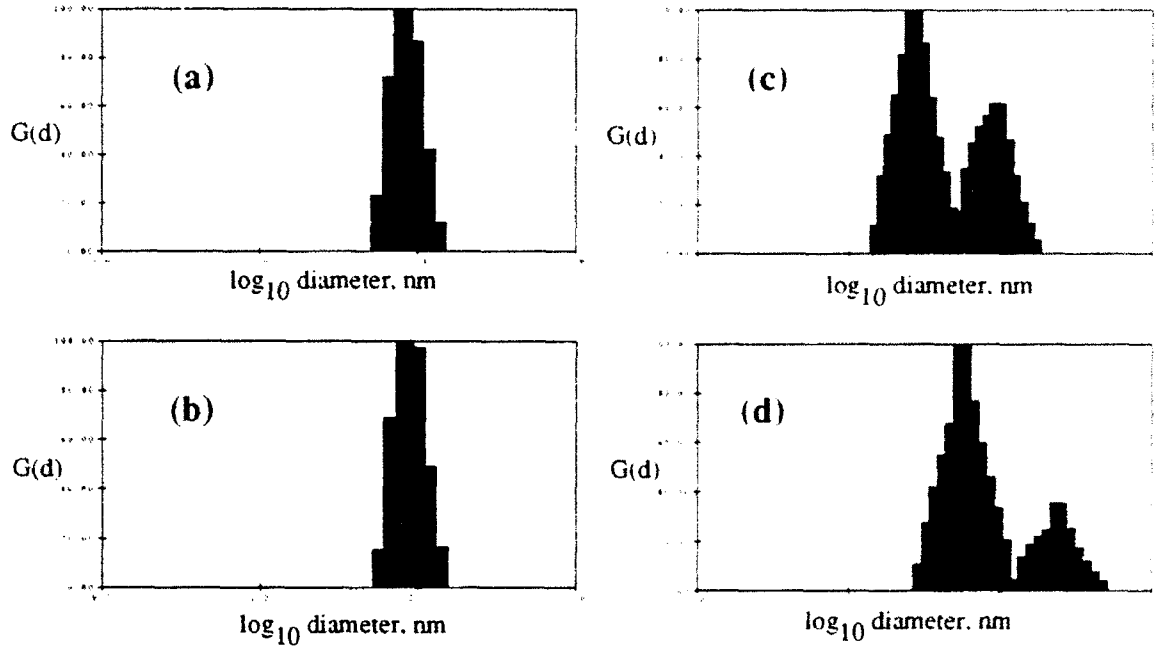

Particle size distributions $G(d)$ *versus* $\log_{10}$ particle diameters (in nm) for: (a) N3M analyzed by the non-negatively constrained least squares (NNLS) routine; (b) BR3M analyzed by NNLS; (c) BI850K analyzed by the exponential sampling (EXPSAM) technique; and (d) BI4M analyzed by EXPSAM.

Figure 9. Particle size distribution results

The analysis of the bimodal samples always yielded a bimodal distribution with the peaks at their approximately expected locations. These correlation functions were analyzed by different data routines, and essentially the same results were obtained. All distributions shown in Figure 9 were analyzed via the exponential sampling technique or the non-negatively constrained least squares analysis, because the other data analysis techniques mentioned in section 1.3.1 (cumulants and double exponential) yield only one or two size values, not a distribution, however the numbers obtained with the other data analyses were consistent with those shown in the figure.

The different data analysis routines appear to produce distributions with their own characteristic shapes (notice the similarities between Figures 9a and 9b, and between Figures 9c and 9d). The Exponential Sampling (EXPSAM) method tended to produce smoother bell-shaped distributions than the non-negatively constrained least squares (NNL) analyses, which had a more pointed shape. In the case of the bimodal distributions, the NNL routines always produced two distinct peaks which did not overlap, while the EXPSAM results were more continuous over the entire size distribution, as shown in Figures 9c and 9d.

3.2.3 Molecular Weight Distributions

Molecular weight distributions (MWD's) were determined for the four polymer samples depicted in Figure 9 by first transforming the PSD's to distributions of linewidths (Γ's) via the Stokes-Einstein equation (eq. 4) and then transforming the linewidth distributions to MWD's via the equations given in section 1.2.1.3. All the MWD transformations were performed on PSD's determined via the NNL analysis routine, because the MWD's produced from the EXP-SAM technique were not smooth.

Figure 10 shows the results of the molecular weight transformations. The values of the parameters k_D, k_T, k_T', b and b' affect the shape of the resultant distribution as well as the numbers derived from it (radius of gyration and molecular weight averages). As a first attempt at a transformation, values of k_D were estimated and the experimental values of the other four parameters (as reported in Equations 26 and 27) were used. These *a priori* values produced a realistic MWD for only one of the particle size distrubutions (N3M). All the other distributions required some parameter adjustment to produce a smooth distribution with meaningful numbers. A computer program was written to calcualte a MWD and the resultant averages (R_g, M_w, M_n) for a given set of adjustable parameters.

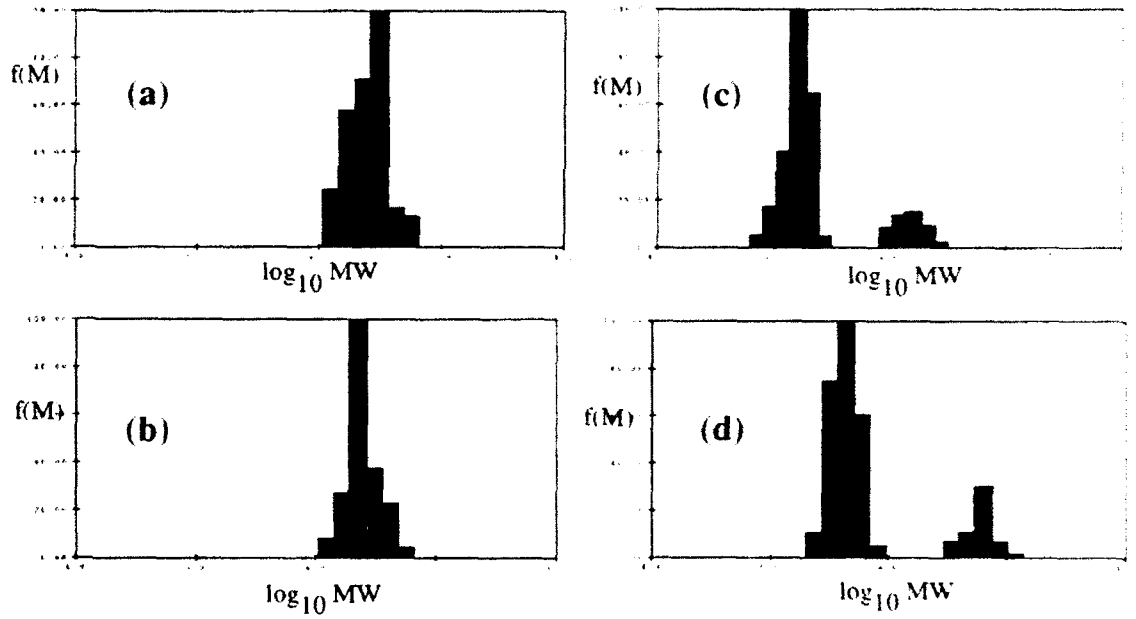

Molecular weight distributin f(M) versus $\log_{10}$ molecular weight for : (a) N3M ; (b) BR3M; (c) BI850K; and (d) BI4M. *All were transformed from* PSD's computed via the NNL data analysis routine.

Figure 10. Molecular weight distribution results

The dynamic parameters k_T and b, transform the diffusion coefficients into molecular weight values, and thus have a significant effect on the distribution. For the bimodal samples, increasing b from the measured value of 0.563 to 0.58 (which is more consistent with the literature) produced a smoother distriubtion. The BI850K sample required a furthe· minor adjustment of

parameter k_T to 3.1 x 10^{-4} (from 3.18 x 10^{-4}) to produce the final distribution. The static parameters k_T' and b', which transform molecular weight values into radii of gyration, only affected the final R_g values, so they were left at their experimentally determined values.

The second virial coefficient for diffusion, k_D, transforms the diffusion coefficients measured at finite concentrations to infinite dilution values, D_o. Of the four distributions shown in Figs. 9 and 10, k_D was only measured for sample N3M, and this value of k_D was used unchanged in the molecular weight transformation process. The other k_D values were determined by trial and error using a value estimated from Figure 7 as a starting point. The final values were all less than those estimated from the figure. For sample BR3M, the value of k_D was decreased by about 30%, and for the two bimodal polymers, approximately 15% each. Incidentally, the measured value of k_D for sample N3M is about 30% lower than the value calculated from Figure 7.

Table 4 contains the molecular weights and radii of gyration calculated from the distributions shown in Figure 10. The numbers calculated from the unimodal distributions matched the experimental data better than the two bimodal samples. An attempt was made to use two different k_D values in the molecular weight transformation process for the bimodal samples, but there was little effect on the final distribution.

Table 4. Parameters calculated from molecular weight distributions

	M_w (x 10^{-6})	M_w/M_n	R_g, nm	peak MW's (x 10^{-6})	Adjusted Parametes
N3M	2.99 (+ 3)	1.14	86.7 (- 3)	3.08	none
BR3M	2.84 (-10)	1.11	88.1 (- 4)	2.25	$k_D \Rightarrow 250$
BI850K	1.21 (+44)	2.96	55.0 (-13)	0.161 (- 4), 1.620 (-24)	$k_D \Rightarrow 90$ $b' \Rightarrow 0.58$ $k_T' \Rightarrow 3.1E\text{-}4$
BI4M	5.16 (+26)	3.43	128.3 (- 1)	0.437 (-56), 6.37 (-32)	$k_D \Rightarrow 350$ $b' \Rightarrow 0.58$
Numbers in parentheses indicate percent differences from expected values					

One interesting thing to note for both bimodal samples is that even though the calculated overall weight-average molecular weights are significantly higher than expected, the peak molecular weights for each of the components are lower than expected. This implies that either the two molecular weight fractions are broad distribution with a high molecular weight tail, or that the estimate of the fraction of the larger molecular weight component is too high. Estimates of the polydispersity (M_w/M_n) of each of the fractions are about 1.05, thus ruling out the first possibility. The mole fraction of each component can be determined by dividing the sum of the $f(M_i)$'s for each component by the sum of the $f(M_i)$'s for the entire distribution. Using this approach, the mole fraction of the lower molecular weight component is 81% for the BI4M sample, and 82% for the BI850K sample. Converting the original weight fractions of each component (see Table 1) to mole fractions, the lower molecular weight components should be 94% and 96%,

respectively. The cause of this skewing of the distribution toward the higher molecular weight components is probably caused by the inherent bias of light scattering toward the higher molecular weight species.

4. Conclusions

The static light scattering experiments were straightforward, and are reasonably consistent with literature vales. Differences in the refractive index increment, and the Rayleigh ratio of the calibration liquid used in the data analysis could account for the differences. These values are often not published with the light scattering data.

Due to the large variability in the published DLS data for toluene solutions of polystyrene, it is clear that the technique of DLS for even a simple analysis of diffusion coefficients is not a mature field, and experimental data do not always correlate with theoretical predictions. The reason for the large discrepancy in published data is probably due to the fact that the dynamic light scattering experiment is not easy from an experimental point of view, or from the data interpretation side.

For example, the selection of the delay time ($\Delta\tau$) to be used when collecting data for the autocorrelation function affects the shape of the correlation function, and thus the numbers that are derived from the data analysis. For systems with large polydispersity, the use of multiple sample times is recommended to incorporate all possible relaxations, particularly when the number of hardware channels (N) is limited. (Multiple sample times were used for the analysis of sample BI4M.) If multiple sample times are used, and too large a range of sample times is incorporated, information on the larger particles can be lost, whereas if the range of sample times is too short, the information on the smaller particles is sacrificed. Another experimental parameter that affects the results of a DLS experiment is the number of samples used to obtain the correlation function, *i.e.*, the length of time that data is collected. For systems with high scattering power, the experiment does not have to be run as long to accumulate the same number of samples as from an experiment in which the scattering is not as great. Obviously, the more samples that are accumulated in a given experiment, the smoother the correlation function will be, and the more precise the data generated from that experiment will be; however a practical time limit for the data collection must be set. Sometimes a shorter experiment duration is desirable; for instance, the longer the experiment is run, the greater the chance that a spurious dust particle will diffuse into the scattering center, or that the environmental conditions (temperature, humidity, laser intensity, etc.) will change.

Section 1.3.1 briefly describes some data analysis routines which are commonly in use for analyzing correlation functions. Many other methods have been used, and are currently under development - in fact, much of the current DLS literature is devoted to developing new mathematical treatments of this data, and of assessing the accuracy of current methods. Thus, the analysis of DLS data is still an area of active research.

In conclusion, DLS is well suited to measure the dynamic properties of a monodisperse polymer solution, such as translational diffusion, and hydrodynamic radii which when coupled with information from static light scattering, provides a complete dilute solution analysis of a polymer in a given solvent. Indeed, several researchers[20-22] are developing combined static and dynamic light scattering spectrometers so that the static and dynamic parameters may be obtained from the same experiment.

Conversion of an experimentally determined linewidth distribution to a distribution of molecular weights is possible if the parameters k_D, k_T, k_T', b and b' are known or can be estimated, and accurate values of M_w and R_g are available from static light scattering measurements. Using DLS to extract information on the polydispersity of a polymer sample should be limited to determination of a mean value, and possibly one or two moments about that mean, due to the inherent difficulty of extracting a unique linewidth distribution from an experimental correlation function. Unimodal distributions can be distinguished from bimodal distributions if the two species are at least a decade apart (more closely spaced distributions may be distinguishable under certain conditions), but extraction of detailed information about the individual fractions is probably unreliable.

5. References

1. B.J. Berne, R. Pecora, *Dynamic Light Scttering with Applications to Chemistry,Biology, and Physics*, John Wiley & Sons, New York, 1976. (Chapter 1, and references therein.)
2. D. McIntyre, F. Gornick, Eds., *Light Scattering from Dilute Polymer Solutions*, Gordon and Breach Science Publishers, New York, 1964.
3. B. Chu, *Ann. Rev. Phys. Chem.* **2507**, 145 (1970).
4. G.D. Patterson in *Dynamic Light Scattering: Applications of Photon Correlation Spectroscopy*, R. Pecora, Ed., Plenum Press, New York, 1985.
5. B.B. Weiner in *Modern Methods of Particle Size Analysis*, John Wiley & Sons, New York, 1984.
6. D.W. Schaefer, C.C. Han in Ref. 4.
7. B. Chu, A. DiNapoli in Ref. 5.
8. M. Doi, S.F. Edwards, *The Theory of Polymer Dynamics*, Oxford University Press, New York, 1988; Chapter 4.
9. A. Rudin, *The Elements of Polymer Science and Engineering*, Academic Press, New York, 1982.
10. R.S. Stock, W.H. Ray, *J. Polym. Sci.: Pol. Phys. Ed.* **23**, 1393 (1985).
11. D.E. Koppel, *J. Chem. Phys.* **57**, 4814 (1972).
12. N. Ostrowsky, D. Sornette, P. Parker, E.R. Pike, *Opt. Acta* **28**, 1059 (1981).

13. E.F. Grabowski, I.D. Morrison, in *Measurement of Suspended Particles by Quasielastic Light Scattering*, B.E. Dahneke, Ed., Wiley, New York, 1983, p. 199.

14. G.D Phillies, *J. Appl. Poly., Appl. Polym. Symp* **43,** 275 (1989).

15. M. Adam, M. Delsanti, *Macromolecules*, **18** 1760 (1985).

16. G.C. Berry, *J. Chem. Phys.* **44,** 4550 (1966).

17. M.B. Huglin, S.J. O'Donohue, M.A. Radwan, *Eur. Polym. J.* **6,** 543 (1989).

18. W. Kaye, J.B. McDaniel, *Appl. Optics* **13,** 1934 (1974).

19. B. Appelt, G. Meyerhoff, *Macromolecules* **13,** 657(1980).

20. S. Bantle, M. Schmidt, W. Burchard, *Macromolecules* **15,** 1604 (1982).

21. K. Huber, S. Bantle, P. Lutz, W. Burchard, *Macromolecules* **18,** 1461 (1985).

22. T.A.P. Seery, J.A. Shorter, E.J. Amis, *Polymer* **30,** 1197 (1989).

23. B.K. Varma, Y. Fujita, M. Takahashi, T. Nose, *J. Polym. Sci. Polym. Phys. Ed.* **22,** 1781 (1984).

24. S. Park, T. Chang, I.H. Park, *Macromolecules* **24,** 5729 (1991).

25. G.V. Schulz, M. Lechner, in *Light Scattering from Polymer Solutions*, M.B. Huglin, Ed., Academic Press, New York, 1972.

26. H. Yamakawa, *Modern Theory of Polymer Solutions*, Harper & Row, New York, 1971.

27. M.E. McDonnell, A.M. Jamieson, *J. Macromol. Sci. - Phys.* **B13,** 67 (1977).

28. M. Ranamathan, M.E. McDonnell, *Macromolecules* **17,** 2093 (1984).

DISTRIBUTION LIST

No. of Copies	To
1	Office of the Under Secretary of Defense for Research and Engineering, The Pentagon, Washington, DC 20301
	Director, U.S. Army Research Laboratory, 2800 Powder Mill Road, Adelphi, MD 20783-1197
1	ATTN: AMSRL-OP-CI-A
	Commander, Defense Technical Information Center, Cameron Station, Building 5, 5010 Duke Street, Alexandria, VA 22304-6145
1	ATTN: DTIC-FDAC
1	MIA/CINDAS, Purdue University, 2595 Yeager Road, West Lafayette, IN 47905
	Commander, Army Research Office, P.O. Box 12211, Research Triangle Park, NC 27709-2211
1	ATTN: Information Processing Office
	Commander, U.S. Army Materiel Command, 5001 Eisenhower Avenue, Alexandria, VA 22333
1	ATTN: AMCSCI
	Commander, U.S. Army Materiel Systems Analysis Activity, Aberdeen Proving Ground, MD 21005
1	ATTN: AMXSY-MP, H. Cohen
	Commander, U.S. Army Missile Command, Redstone Arsenal, AL 35809
1	ATTN: AMSMI-RD-CS-R/Doc
	Commander, U.S. Army Armament, Munitions and Chemical Command, Dover, NJ 07801
2	ATTN: Technical Library
	Commander, U.S. Army Natick Research, Development and Engineering Center, Natick, MA 01760-5010
1	ATTN: Technical Library
	Commander, U.S. Army Satellite Communications Agency, Fort Monmouth, NJ 07703
1	ATTN: Technical Document Center
	Commander, U.S. Army Tank-Automotive Command, Warren, MI 48397-5000
1	ATTN: AMSTA-ZSK
1	AMSTA-TSL, Technical Library
	Commander, White Sands Missile Range, NM 88002
1	ATTN: STEWS-WS-VT
	President, Airborne, Electronics and Special Warfare Board, Fort Bragg, NC 28307
1	ATTN: Library
	Director, U.S. Army Ballistic Research Laboratory, Aberdeen Proving Ground, MD 21005
1	ATTN: SLCBR-TSB-S (STINFO)
	Commander, Dugway Proving Ground, UT 84022
1	ATTN: Technical Library, Technical Information Division
	Commander, Harry Diamond Laboratories, 2800 Powder Mill Road, Adelphi, MD 20783
1	ATTN: Technical Information Office
	Director, Benet Weapons Laboratory, LCWSL, USA AMCCOM, Watervliet, NY 12189
1	ATTN: AMSMC-LCB-TL
1	AMSMC-LCB-R
1	AMSMC-LCB-RM
1	AMSMC-LCB-RP
	Commander, U.S. Army Foreign Science and Technology Center, 220 7th Street, N.E., Charlottesville, VA 22901-5396
3	ATTN: AIFRTC, Applied Technologies Branch, Gerald Schlesinger
	Commander, U.S. Army Aeromedical Research Unit, P.O. Box 577, Fort Rucker, AL 36360
1	ATTN: Technical Library

No. of Copies	To
	Commander, U.S. Army Aviation Systems Command, Aviation Research and Technology Activity, Aviation Applied Technology Directorate, Fort Eustis, VA 23604-5577
1	ATTN: SAVDL-E-MOS
	U.S. Army Aviation Training Library, Fort Rucker, AL 36360
1	ATTN: Building 5906-5907
	Commander, U.S. Army Agency for Aviation Safety, Fort Rucker, AL 36362
1	ATTN: Technical Library
	Commander, Clarke Engineer School Library, 3202 Nebraska Ave., N. Ft. Leonard Wood, MO 65473-5000
1	ATTN: Library
	Commander, U.S. Army Engineer Waterways Experiment Station, P.O. Box 631, Vicksburg, MS 39180
1	ATTN: Research Center Library
	Commandant, U.S. Army Quartermaster School, Fort Lee, VA 23801
1	ATTN: Quartermaster School Library
	Naval Research Laboratory, Washington, DC 20375
1	ATTN: Code 5830
2	Dr. G. R. Yoder - Code 6384
	Chief of Naval Research, Arlington, VA 22217
1	ATTN: Code 471
	Commander, U.S. Air Force Wright Research & Development Center, Wright-Patterson Air Force Base, OH 45433-6523
1	ATTN: WRDC/MLLP, M. Forney, Jr.
1	WRDC/MLBC, Mr. Stanley Schulman
	NASA - Marshall Space Flight Center, MSFC, AL 35812
1	ATTN: Mr. Paul Schuerer/EH01
	U.S. Department of Commerce, National Institute of Standards and Technology, Gaitherburg, MD 20899
1	ATTN: Stephen M. Hsu, Chief, Ceramics Division, Institute for Materials Science and Engineering
1	Committee on Marine Structures, Marine Board, National Research Council, 2101 Constitution Avenue, N.W., Washington, DC 20418
1	Materials Sciences Corporation, Suite 250, 500 Office Center Drive, Fort Washington, PA 19034
1	Charles Stark Draper Laboratory, 555 Technology Square, Cambridge, MA 02139
	Wyman-Gordon Company, Worcester, MA 01601
1	ATTN: Technical Library
	General Dynamics, Convair Aerospace Division P.O. Box 748, Forth Worth, TX 76101
1	ATTN: Mfg. Engineering Technical Library
	Plastics Technical Evaluation Center, PLASTEC, ARDEC Bldg. 355N, Picatinny Arsenal, NJ 07806-5000
1	ATTN: Harry Pebly
1	Department of the Army, Aerostructures Directorate, MS-266, U.S. Army Aviation R&T Activity - AVSCOM, Langley Research Center, Hampton, VA 23665-5225
1	NASA - Langley Research Center, Hampton, VA 23665-5225
1	U.S. Army Propulsion Directorate, NASA Lewis Research Center, 2100 Brookpark Road, Cleveland, OH 44135-3191
1	NASA - Lewis Research Center, 2100 Brookpark Road, Cleveland, OH 44135-3191
	Director, Defense Intelligence Agency, Washington, DC 20340-6053
1	ATTN: ODT-5A (Mr. Frank Jaeger)
	Director, U.S. Army Research Laboratory, Watertown, MA 02172-0001
2	ATTN: AMSRL-OP-CI-D, Technical Library
5	Author